Journal of
Materials Chemistry A

Accepted Manuscript

This is an *Accepted Manuscript*, which has been through the RSC Publishing peer review process and has been accepted for publication.

Accepted Manuscripts are published online shortly after acceptance, which is prior to technical editing, formatting and proof reading. This free service from RSC Publishing allows authors to make their results available to the community, in citable form, before publication of the edited article. This *Accepted Manuscript* will be replaced by the edited and formatted *Advance Article* as soon as this is available.

To cite this manuscript please use its permanent Digital Object Identifier (DOI®), which is identical for all formats of publication.

More information about *Accepted Manuscripts* can be found in the **Information for Authors**.

Please note that technical editing may introduce minor changes to the text and/or graphics contained in the manuscript submitted by the author(s) which may alter content, and that the standard **Terms & Conditions** and the **ethical guidelines** that apply to the journal are still applicable. In no event shall the RSC be held responsible for any errors or omissions in these *Accepted Manuscript* manuscripts or any consequences arising from the use of any information contained in them.

Nafion-functionalized electrospun poly(vinylidene fluoride) (PVDF) nanofibers for high performance proton exchange membranes in fuel cells

Hsieh-Yu Li and Ying-Ling Liu

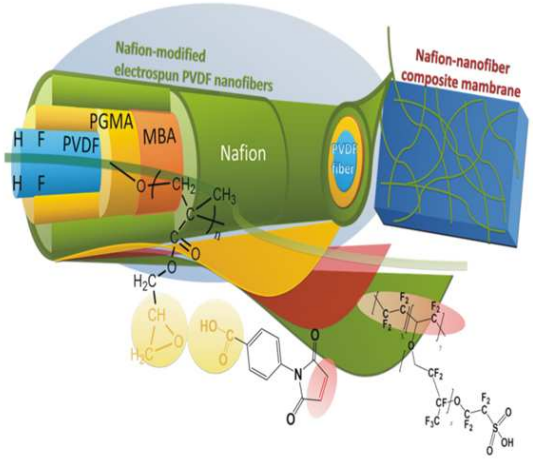

Nafion-functionalized electrospun poly(vinylidene fluoride) nanofibers show high performance in preparation of proton exchange membranes for fuel cells.

Nafion-functionalized electrospun poly(vinylidene fluoride) (PVDF) nanofibers for high performance proton exchange membranes in fuel cells

Hsieh-Yu Li, Ying-Ling Liu*

Department of Chemical Engineering, National Tsing Hua University,

#101, Sec.2, Kuang-Fu Road, Hsinchu 30013, Taiwan.

* All correspondence should be addressed to Professor Ying-Ling Liu

Fax: +886-3-5715408; Tel: +886-3-5711450; E-mail: liuyl@mx.nthu.edu.tw

Abstract

Nafion-functionalized poly(vinylidene fluoride) electrospun nanofibers (PVDFNF-Nafion) has been prepared through a 3-step reaction route. The chemical strcuture of PVDFNF-Nafion is characterized with Fouirier transform Infrared and X-ray photoelectron spectroscopy. Functionalization with Nafion chains improves the interfacial compatbility between the PVDF-based nanofibers and Nafion matrix in formation of PVDFNF-Nafion reinforced Nafion composite membrane (Nafion CM1). Aggregation of Nafion chains on the nanofiber surfaces induces the formation of proton-conducting channels so as to increase the proton conductivity of the Nafion-CM1 membrane. In the H_2/O_2 single cell test, Nafion-CM1 shows a maximum power density of 700 mW cm^{-2} which is higher than the value of 500 mW cm^{-2} recorded with commercial Nafion 212 membrane. The presence of PVDFNF-Nafion also depresses the methanol permeability of the Nafion-CM1 membrane with alternation of the crystalline domains of Nafion. In direct methanol fuel cell tests, the low methanol permeability of Nafion-CM1 makes it could be operated with a 5M methanol as the fuel and exhibit a maximum poewer density of 122 mW cm^{-2}, which is larger than the value (60 mW cm^{-2}) recorded with commercial Nafion 117 membrane at 2M methanol fuel.

Keywords: Nafion; fuel cell; proton exchange membrane; electrospun nanofiber

Introduction

Proton exchange membranes (PEMs) are the key components for hydrogen and direct methanol fuel cells. The preliminary characteristic required for the membranes is high proton conductivity. Research efforts on designs and preparation of PEMs which are capable of exhibiting high proton conductivities under various operation conditions including low relative humidity and high temperatures have been widely reported.[1-5] Consideration of the mechanism of proton transportation through PEMs, formation of continuous proton-conductive domains and channels in PEMs is an effective approach to significantly increase the proton conductivity of the membranes.[6] One of the reported approaches is *in situ* formation of proton-conductive domains through microphase-separation of polyelectrolyte copolymers.[7-11] Controls of domain sizes and morphological patterns with molecular designs of polyelectrolytes have been demonstrated for preparation of PEMs exhibiting high proton conductivity exceeding the values of commercial Nafion-based membranes. Moreover, addition of inorganic nanofillers,[12] including inorganic superacids[13] and sulfonated nanoparticles,[14-16] to PEMs could induce the phase-separated domains in PEMs. In the organic-inorganic composite PEMs, aggregation of acidic groups forms proton-conductive domains and increase the proton conductivity. Compared to the phase-separated domains, long-range proton-conducting channels are even more attractive in preparation of high performance PEMs. The channels could provide continuous hopping pathways for protons transporting through PEMs. Surface-functionalized carbon nanotubes (CNT) have been utilized as effective additives for polyelectrolytes to generate long-range proton-conductive channels in the resulting PEMs.[17-21] In the CNT-modified PEMs, the channels in the length of several micrometers form along with the surfaces of CNT bundles and serve as a superhighway for proton transportation.

Electrospinning is an effective process for fabrication of fibers in submicrometer to

nanometer scale.[22,23] Choi *et al*[24] prepared electrospun polyelectrolyte nanofibers and demonstrated the nanofibers could serve as percolation pathways for ionomers. Successive papers[25-27] reported the application of the nanofibers for preparation of high performance PEMs with non-ionic matrixes. Yao *et al*[28] further demonstrated that sulfated zirconia nanofibers could induce long-range proton-conductive channels in PEMs made with the nanofibers and crosslinked poly(2-acrylamido-2-methylpropane-sulfonic acid) matrix. As a result, PEMs made with polyelectrolyte nanofibers and polyelectrolyte matrix receive research interest with their potential to exhibit enhanced proton conductivity, improved mechanical properties, and high single cell performance.[29-34] Moreover, Tamura and Kawakami[35,36] explored the uses of uniaxially-aligned polyelectrolyte nanofibers in preparation of composite PEMs. The PEMs showed high proton conductivity in the direction parallel to the aligned fibers. The results provide further supports to the ability of nanofibers to induce long-range proton transportation channels in the composite PEMs.

As Nafion is one of the most promising materials for PEMs, composite membranes made with Nafion and nanofibers have been studied.[37-43] Nonionic nanofibers have been utilized for preparation of Nafion-based composite membranes.[37-40] The composite PEMs exhibited reduced proton conductivity due to the decrease in the ion exchange capacity. This drawback could be overcome by using polyelectrolyte-based nanofibers as the reinforcements for the Nafion-based composite PEMs.[41-33] The resulting composite PEMs showed not only increased proton conductivity but also improved mechanical strength and depressed methanol permeability compared to the neat Nafion membrane. On the other hand, Lee *et al*[44] and Bajon *et al*[45] reported their preliminary study on preparation of Nafion electrospun nanofibers for using as the proton-conducting part of the corresponding composite PEMs. Dong *et al*[46] demonstrated that the proton conductivity of Nafion nanofibers in diameters below 400 nm is about 1.5 S cm^{-1}, which is much higher than the

value (about 0.1 S cm^{-1}) recorded with bulk Nafion membrane. The high proton conductivity has been attributed to the anisotropic ionic aggregation in the Nafion nanofibers, in contrast to the isotropic aggregation in the Nafion membrane. The results suggest that use of Nafion electrospun nanofibers and Nafion matrix is a promising approach to prepare high performance PEMs. Utilization of Nafion nanofibers in preparation of Nafion-based composite membranes could improve the interfacial compatibility of the nanofibers and Nafion matrix and enhance the ionic aggregation along the nanofibers. Nevertheless, to our best knowledge this kind of PEMs has not been reported yet, probably due to the difficulty in fabrication of Nafion nanofibers and the relatively poor mechanical properties of the Nafion nanofibers.

Poly(vinylidene fluoride) (PVDF), which has good thermal stability, chemical resistance, mechanical strength, and electrical properties, has been widely utilized for preparation of polyelectrolytes for fuel cells.[9,47,48] In this work, Nafion-functionalized PVDF nanofibers have been prepared and utilized as an alternative of Nafion nanofibers for preparation of nanofiber-reinforced Nafion-based composite membranes. A three-step reaction route has been carried out to chemically incorporate Nafion chains to the surface of PVDF nanofibers (PVDFNF) to improve the interfacial compatibility between the nanofibers and Nafion. Moreover, the Nafion surface layer of the Nafion-functionalized PVDF nanofibers could induce the formation of anisotropic ionic aggregation which could promote proton transportation. The resulting composite membranes have shown attractive properties, including high proton conductivity, good mechanical properties, low methanol permeability, and high dimensional stability, for application in hydrogen and direct methanol fuel cells.

Results and discussion

Preparation of Nafion-functionalized PVDF nanofibers

Electrospun PVDFNF in diameters of about 400 nm have been obtained with an

electrospinning process for preparation of nanofiber-reinforced Nafion composite membranes. To improve the interfacial compatibility between the PVDF nanofibers and Nafion in formation of Nafion-based composite membranes, Nafion has been chemically incorporated onto PVDFNF to result in Nafion-functionalized PVDF nanofibers (PVDFNF-Nafion). As Nafion chains do not possess chemically reactive sites, reactions of Nafion polymer is not easy to carry out. In this work, a novel reaction route has proposed to chemically incorporate Nafion chains to the surfaces of PVDFNF (**Figure 1**). Ozone-treatment could generate peroxide groups in the Nafion chains.[19] Thermal decomposition of the peroxide groups forms highly reactive radicals so as to introduce chemically reactive sites to the Nafion chains. The ozone- and thermally-treated Nafion chains possessing radical groups are reactive toward C=C unsaturated groups.[19,49] Surface functionalization of PVDF nanofibers has been performed with two-step reactions to incorporate some C=C unsaturated groups to the nanofiber surfaces. The first reaction is surface-initiated radical polymerization of glycidylmethacrylate (GMA) from PVDF nanofibers, and the second one is the addition reaction between maleimidobenzoic acid (MBA) and the epoxide groups of the grafted PGMA chains. The maleimide groups anchored on the surfaces of the modified PVDF nanofibers serve as the active sites to react with the radicals-containing Nafion chains. Finally, the Nafion-functionalized PVDF nanofibers (PVDFNF-Nafion) are obtained with the reaction between these two precursors. The amount of PGMA and Nafion chains grafted to the PVDF nanofiber surfaces have been determined with a gravimetric method to be 33 and 65 μg cm^{-2}, respectively.

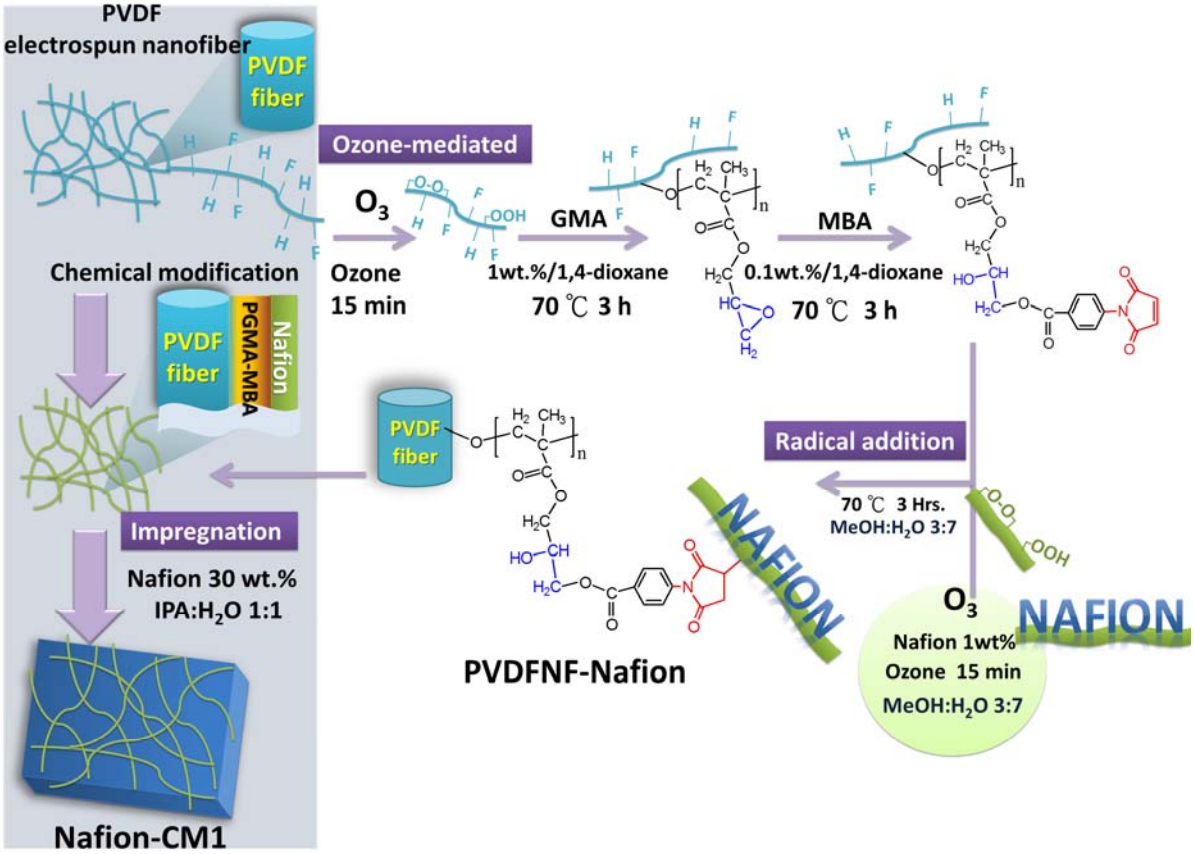

Figure 1. Synthetic route of Nafion-functionalized PVDF nanofibers (PVDFNF-Nafion) and preparation of Nafion-CM1 composite membrane.

The performance of the reactions and the surface structures of the modified nanofibers have been characterized by X-ray photoelectron spectroscopy (XPS). In the wide-scan spectra (**Figure 2a**), the neat PVDFNF sample exhibits only signals arising from carbon and fluoride atoms. Incorporation of PGMA to PVDFNF surfaces results in the appearance of the oxygen atom peak in the spectrum of PVDFNF-PGMA. Similarly, the presence of MBA moieties in the PVDFNF-MBA sample could be characterized with the nitrogen atom peak. Moreover, the Nafion chains incorporated to PVDF nanofibers are characterized with the S signal in the wide-scan XPS spectrum of PVDFNF-Nafion sample. The C_{1s} core-level spectra of the samples provide more information about the chemical structures of the nanofiber surfaces (**Figure 2b**). The peaks at binding energy of 290.9 eV and 286.4 eV correspond to the $\underline{C}F_2$

and $\underline{C}H_2$ groups of PVDF, respectively. These two peaks appear in the C_{1s} core-level spectra of all the PVDF-based nanofiber samples. The C_{1s} core-level XPS spectrum changes with the incorporation of PGMA chains to PVDF nanofibers. As a result, the presence of PGMA chains on the PVDFNF-PGMA surface is characterized with the peaks at 289.0 eV ($\underline{C}$(=O)O), 287.0 eV (epoxide), and 285.0 eV ($\underline{C}$H). Similarly, incorporation of the MBA moieties results in the appearance of the peak at 288.3 eV (imide group) and the decrease in the intensity of the epoxide peak at 287.0 eV, as shown in the C_{1s} core-level XPS spectrum of PVDFNF-MBA. After functionalization with Nafion, PVDFNF-Nafion exhibits a very different C_{1s} core-level spectrum, which demonstrates the $\underline{C}F_3$ peak at 294.1 eV, the $\underline{C}F_2\underline{C}F$ peak at about 292.0, and the $\underline{C}F_2SO_3H$ peak at 288.6 eV. The peaks are different with the $\underline{C}F_2$ absorption of PVDF chain (at about 290.9 eV) and correspond to the chemical structure of Nafion. **Figure 2c** collects the FTIR spectra of the prepared nanofibers to provide further supports to the successful surface functionalization of the samples. PVDFNF exhibits typical absorption peaks of -CF_2 groups at about 1175 cm^{-1}. The PGMA chains of PVDFNF-PGMA demonstrate the absorptions of epoxide groups and about 915 cm^{-1} and -C=O linkages of ester groups at 1725 cm^{-1}. Reaction of MBA with the epoxide groups of PVDFNF-GMA results in the decrease in the absorption intensity of epoxide groups and the appearance of the C=C linkages of imide groups at 1605 cm^{-1} and the absorption of phenyl group at 1503 cm^{-1} in the spectrum of PVDFNF-MBA. Moreover, PVDFNF-Nafion shows the absorption of -SO_3H groups at 1053 cm^{-1} which supports to the Nafion chains are grafted onto the nanofiber surfaces.

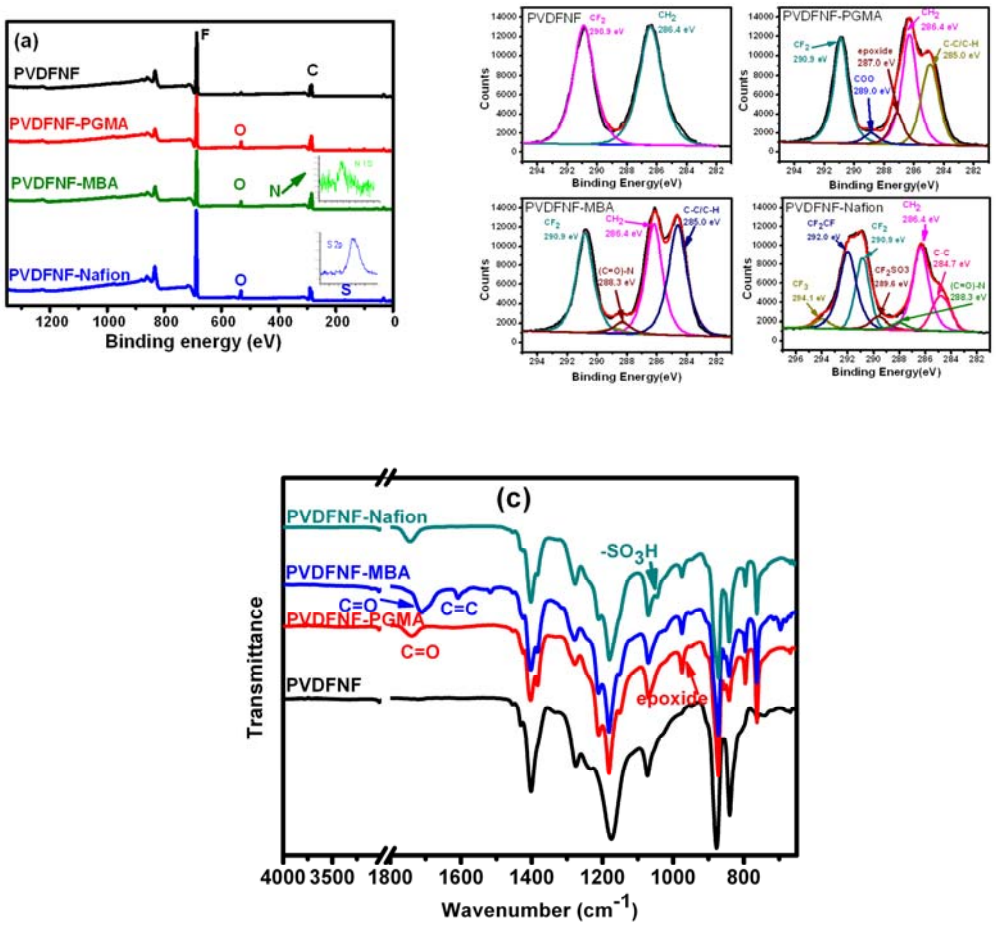

Figure 2. Characterization of surface-functionalized PVDF nanofibers. (a) XPS wide-scan spectra, (b) XPS C_{1s} core-level spectra, and (c) FTIR spectra.

The PVDF-based nanofiber samples are applied to scanning electron microscopy (SEM) and the obtained micrographs are collected in **Figure 3**. The neat electrospun PVDF nanofibers are homogenous and in diameters of about 400 nm. After incorporation of PGMA chains, the nanofibers become relatively soft and large. The morphology of PVDFNF-PGMA indicates the sample might be somewhat swollen with the solvent (1,4-dioxane) used in the reaction procedure. The nanofibers become relatively firm after being incorporated with Nafion chains as the nanofibers are less swollen in the solvent (water/methanol mixture) used for Nafion reaction. PVDFNF-Nafion exhibits similar morphology in SEM, to demonstrate that

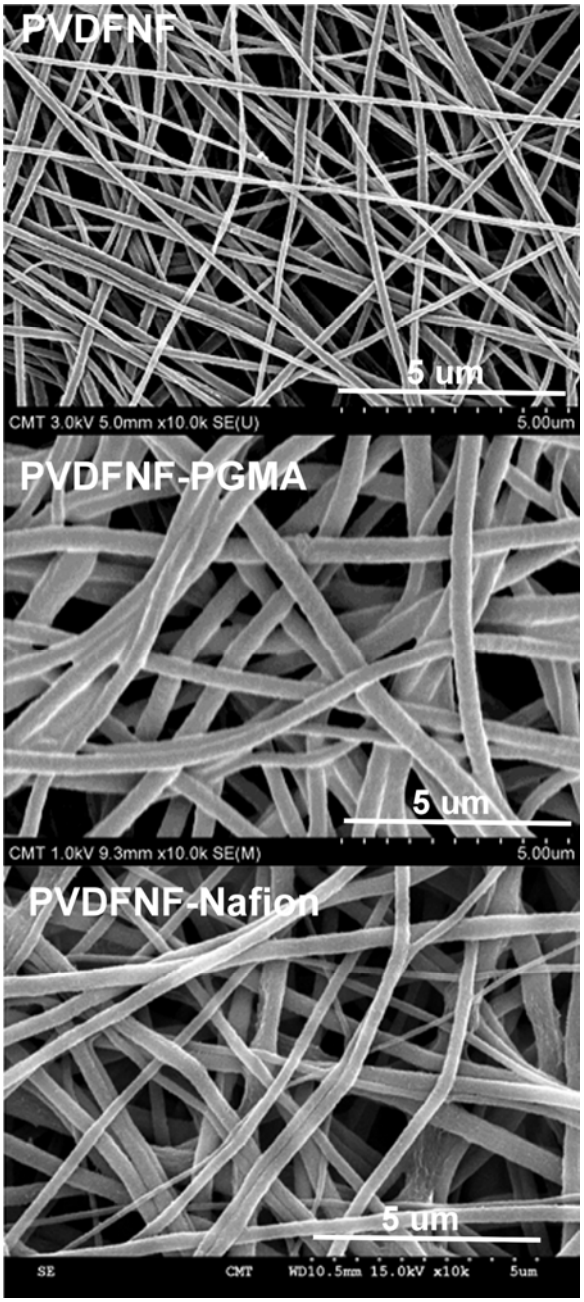

Figure 3. SEM micrographs of surface-functionalized PVDF nanofibers.

the surface functionalization process does not change the nanofiber structures. Nevertheless, the electrospun nanofibers have been obtained in a range of diameters. As a result, the diameter change of the individual nanofiber before and after surface modification could not be read from the SEM micrographs. The neat PVDFNF sample shows a surface water contact angle of about 139^{o}, which is much higher than the contact angle recorded with the

corresponding PVDF plain film. The increase in the surface hydrophobicity of PVDF nanofibers results from the porous structure of the mat.[45] The water contact angle of PVDFNF-PGMA decreases to 115° associating with the incorporation of the relatively hydrophilic PGMA chains. The water contact angle recorded with PVDFNF-Nafion is 134°. The hydrophobic fluoro-containing groups which have relatively low surface free energy might diffuse toward surface to result in a hydrophobic surface of Nafion, as Nafion plain film shows a water contact angle of about 110°. Like PVDFNF, the nanofiber structure of PVDFNF-Nafion further enhances its hydrophobicity with an increase in the water contact angle from 110° to 134°.

Composite membranes of Nafion and PVDFNF-Nafion

The Nafion-based composite membrane with PVDFNF-Nafion as the reinforcement is coded as Nafion-CM1 and has been prepared with an impregnation process. The composite membrane using the neat PVDFNF as the reinforcement is coded as Nafion-CM2. The plain recasting Nafion membrane (coded as Nafion-RC) is also prepared for comparison. All the membranes have a thickness of about 90 μm. The weight fractions of the nanofibers in the composite membranes are about 10 wt% being determined with gravimetric measurements. The membrane thickness and nanofiber contents were controlled by the amounts of nanofiber and Nafion solution used in the membrane fabrication process. **Figure 4** collects the cross-sectional SEM micrographs of the membranes. In contrast to the dense and homogeneous morphology of the Nafion-RC membrane, nanofibers appear clearly in the SEM micrographs of the composite membranes. For Nafion-CM1, the Nafion layer grafted on the nanofiber surfaces improves the interfacial interaction and compatibility between the nanofiber reinforcement and the Nafion matrix. As a result, the fibers embed in the Nafion matrix and tend to lie perpendicular to the cross-sectional plane of the membrane. In contrast, the interfacial compatibility between the components of Nafion-CM2 is relatively poor as

there is not strong interaction between the neat PVDFNF nanofibers and the Nafion matrix. The fibers in Nafion-CM2 membrane are separated from the matrix and randomly appear in the cross-sectional plane. The results indicate that Nafion-functionalization of the PVDF nanofibers is critical fto improve the quality of the Nafion-based composite membranes.

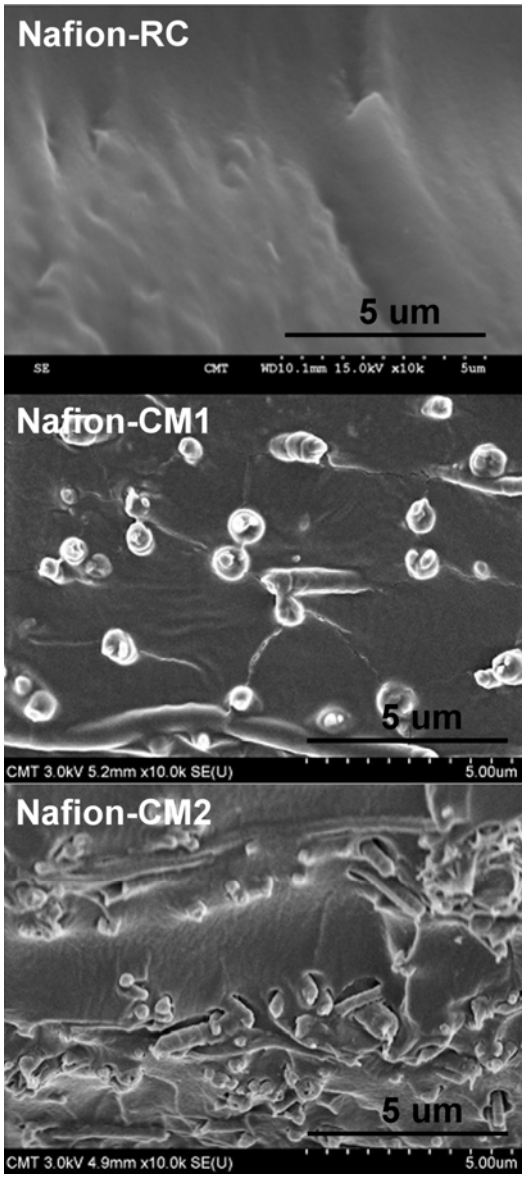

Figure 4. SEM micrographs of Nafion-based membranes at a cross-sectional view.

The mechanical properties of the membranes in dry state were measured with an Instron (**Figure 5a**). From the data collected in **Table 1**, Nafion-CM1 membrane has an elastic moduli up to 1,840 MPa and a maximum stress of 12 MPa. Compared to Nafion-RC,

Nafion-CM1 exhibits 43% increase in Young's modulus, 48% increase in strength at break, and 100% increase in elongation at break. The mechanical properties of Nafion-CM1 membrane is also superior over that recorded with the commercial Nafion 212 membrane (Young's modulus: 1,190 MPa; maximum stress: 14.4 MPa). PVDFNF-Nafion has shown a great reinforcing effect on the Nafion-based membrane. Nevertheless, the mechanical properties of Nafion-CM2 membrane are not as good as those of Nafion-CM1 membrane. The results are reasonably attributed to the relatively poor compatibility between the nanofiber reinforcement and the Nafion matrix for Nafion-CM2. The difference in the interfacial compatibility of the composite membranes could also be observed with the morphological difference of the samples before and after Intrson tests (**Figure 5b**). Nafion-CM1 and Nafion-CM2 are both transparent before Instron tests. Nevertheless, Nafion-CM2 becomes opaque after elongation. The opaque Nafion-CM2 sample implies the occurrence of phase-separation between Nafion matrix and the PVDFNF reinforcement during elongation due to the lack of strong interfacial interaction and compatibility between PVDFNF and Nafion matrix. **Figure 5c** shows the SEM micrographs of the Nafion composite membranes after Instron tests. In both the surface and cross-sectional images, Nafion-CM1 shows high interfacial strength to prevent serious separation and delamination under stress. Nafion-functionalization of PVDF nanofibers improves the interfacial compatibility and enhances the interaction between the two components of Nafion-CM1 membranes, so as to prevent the phase-separation in elongation of the membrane.

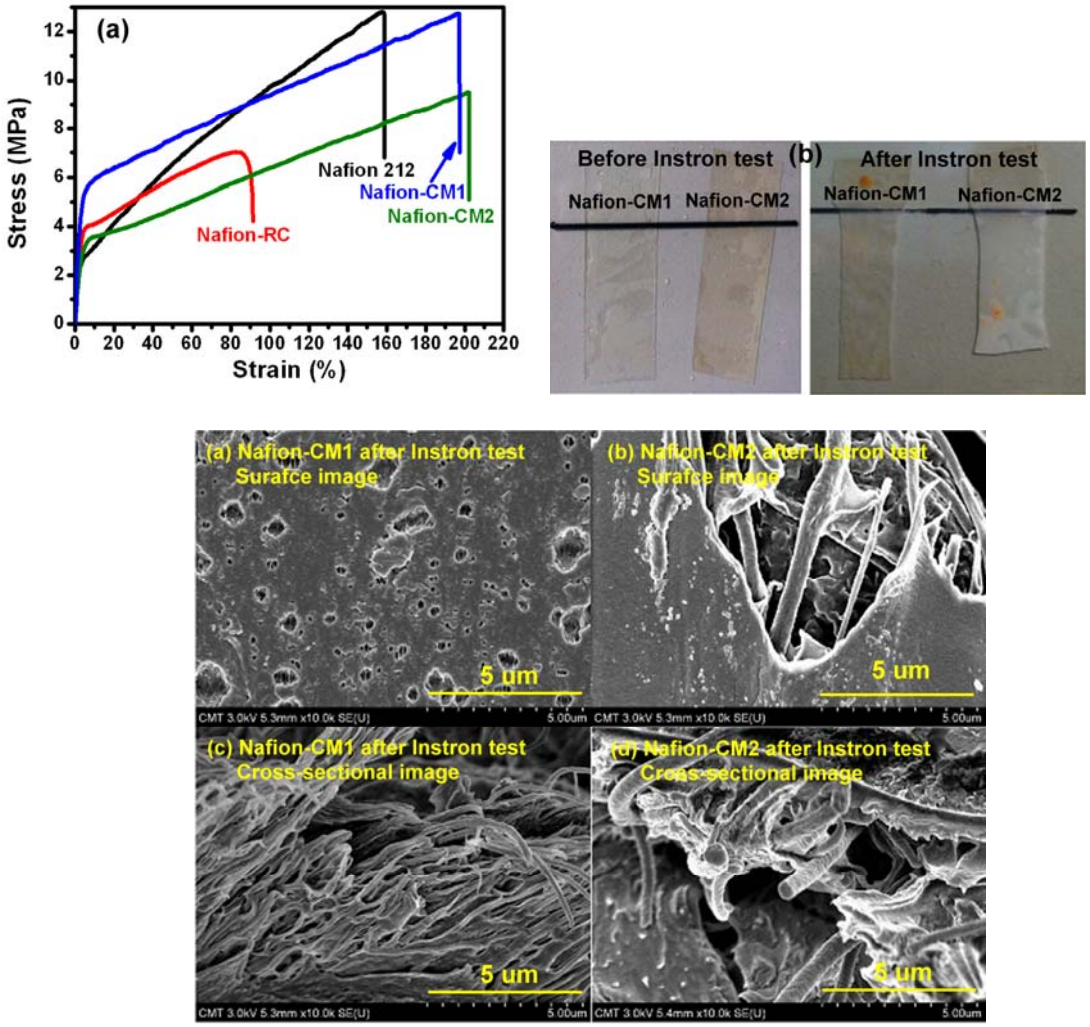

Figure 5. (a) Stress-strain curves of Nafion-based membranes; (b) Pictures of the Nafion-CM1 and Nafion-CM2 samples before and after Instron tests; and (c) SEM micrographs of the Nafion-CM1 and Nafion-CM2 samples before and after Instron tests.

Table 1. Properties of the Nafion-based membranes in this work.

Membrane	Thickness (μm)	Water uptakes			Mechanical properties		
		Water uptakes (wt%)	In plane dimensional change (%)	Through plane dimensional change (%)	Young's modulus (MPa)	Elongation at break (%)	Stress at break (MPa)
Nafion-RC	90	22.7±1.4	10.1±0.5	44.1±1.7	1280±170	116±24	8.1±0.7
Nafion-CM1	90	26.9±1.3	8.1±0.9	8.7±1.0	1840±220	230±23	12.0±0.7
Nafion-CM2	90	24.8±1.7	8.9±1.3	9.9±0.6	1150±30	185±30	7.7±0.9
Nafion 212	60	23.0±0.6	7.7±0.3	45.4±1.4	1190±80	185±18	14.4±1.7

The water uptake of Nafion-CM1 is about 27%, which is larger than the water uptakes of Nafion 212 and Nafion-RC membranes (**Table 2**). The increase in the water uptake for the composite membrane could result from the aggregation of protogenic groups of Nafion on the PVDFNF-Nafion nanofiber surfaces due to the interaction of the sulfonic acid groups. The result is coincident to the previously reported data and might indicate the formation of long-range ionic pathways along the nanofiber surfaces in lengths of micrometers.[41] Nafion-CM2 shows a water uptake of about 25 %, which is still larger than the value recorded with Nafion-RC membrane. As PVDFNF is relatively hydrophobic, the increased water uptake of Nafion-CM2 membrane could be attributed to the micropores in the membrane due to the relatively poor interfacial compatibility between PVDFNF reinforcement and Nafion matrix. It is noteworthy that the increase in the water uptake of Nafion-CM1 does not result in a decrease in the dimensional stability of the membrane, as the water molecules aggregate along the PVDFNF surfaces which are dimensionally stable upon hydration. The in-plane dimensional change of Nafion-CM1 upon water swelling is about 8 %, which is smaller than the value of Nafion-RC (10%) and close to the data measured with Nafion 212 (8%). Moreover, formation of Nafion composite membranes with the nanofibers could dramatically enhance the z-direction dimensional stability of the Nafion-based membranes. Compared to the z-direction dimensional change of Nafion 212 and Nafion-RC membranes (about 44-45%), Nafion-CM1 membrane exhibits a value of only about 9%. The reduction of the z-direction dimensional change enhances the volume stability of Nafion-CM1 membrane and its reliability for the cycling fuel cell operation.[30]

Table 2. Hydrogen fuel cell tests of the Nafion-based membranes at 65 °C.

Membrane	Proton conductivity at 20 °C (mS cm^{-1})	Activation energy of proton conduction[a] (kJ mol^{-1})	H_2/O_2 fuel cell test			H_2/air fuel cell test		
			OCV (V)	Maximum power density (mW cm^{-2})	Current density at 0.6 V (mA cm^{-2})	OCV (V)	Maximum power density (mW cm^{-2})	Current density at 0.4 V (mA cm^{-2})
Nafion-RC	22	8.5	0.84	410	440	0.82	170	360
Nafion-CM1	60	3.0	0.89	700	960	0.89	240	470
Nafion-CM2	36	8.4	0.88	530	470	0.88	210	450
Nafion 212	42	9.4	0.84	500	340	0.82	170	360

[a] Value calculated from the proton conductivity in the temperatures between 30-60 °C.

Morphological nanostructure, proton conductivity, and methanol permeability

The nanophase separation of Nafion-based membranes has been studied and correlated to their ionic domains.[7,51,52] Nafion-based membranes exhibit two peaks in small-angle X-ray scattering (SAXS) pattern, one appears in the low *q* region corresponding to the long-range order domains and the other one is in the high *q* region ascribing to the distribution of ionic clusters.[51,52] **Figure 6** shows the SAXS patterns of the Nafion-based membranes prepared in this work. The commercial Nafion 212 membrane shows an ionomer peak at a relatively low *q* value, compared to the peak positions of the recast Nafion-based membranes. Nevertheless, peak shifts are not observed with Nafion-CM1 and Nafion-CM2, indicating that the presence of the nanofiber mats does not alter the ionic cluster domain sizes of the Nafion-based membranes. As the increases in the domain sizes has been demonstrated to effectively contribute to the increases in the proton conductivities,[52] the effect could not be seen in the cases of Nafion-CM1 and Nafion-CM2 membranes. Nevertheless, the nanofiber mats might alter the long-period lamellar crystalline domains of Nafion to result in the changes in the low-*q* peaks. The nanofibers could induce the nucleation effect of Nafion chains so as to reduce the crystalline cluster sizes of Nafion matrix from about 7.6 nm (Nafion-RC) to 5.8 nm (Nafion-CM1) and increase the fraction of crystalline region. The results contribute to a distortion of ionic channels so as to reduce the fuel permeation ability through the composite

membranes (to be discussed later).

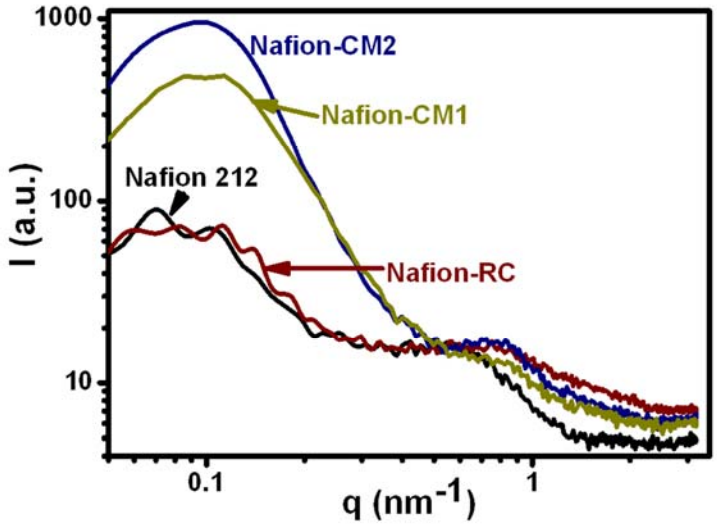

Figure 6. Small angle X-ray scattering spectra of Nafion-based membranes.

The above results suggest that the Nafion-CM1 membrane might not possess enlarged ionic clusters contributing to ion transportation. Nevertheless, as shown in **Figure 7**, the proton conductivity measured with Nafion-CM1 at 20 ^{o}C is about 60 mS cm^{-1}, which is higher than the values recorded with Nafion-RC (22 mS cm^{-1}) and Nafion 212 (42 mS cm^{-1}). The presence of PVDFNF-Nafion nanofibers results in a 2.7-fold increase in the proton conductivity of the Nafion-based membrane. The Nafion-modified nanofibers have strong interactions with the Nafion matrix. As the interaction might mediate with water molecules,[52] the relatively high water uptake recorded with Nafion-CM1 promotes the above-mentioned interaction. The water-mediated domains along the Nafion-modified nanofiber surfaces serve as continuous pathways for proton transportation, so as to increase the proton conductivity. Moreover, the activation energy for proton conduction has been calculated from Arrhenius equation. Compared to Nafion-RC, Nafion-CM1 still shows a relatively low value of activation energy, indicate that the PVDFNF-Nafion nanofibers are capable to enhance the proton conduction characteristics of the Nafion-CM1 membrane.[31]

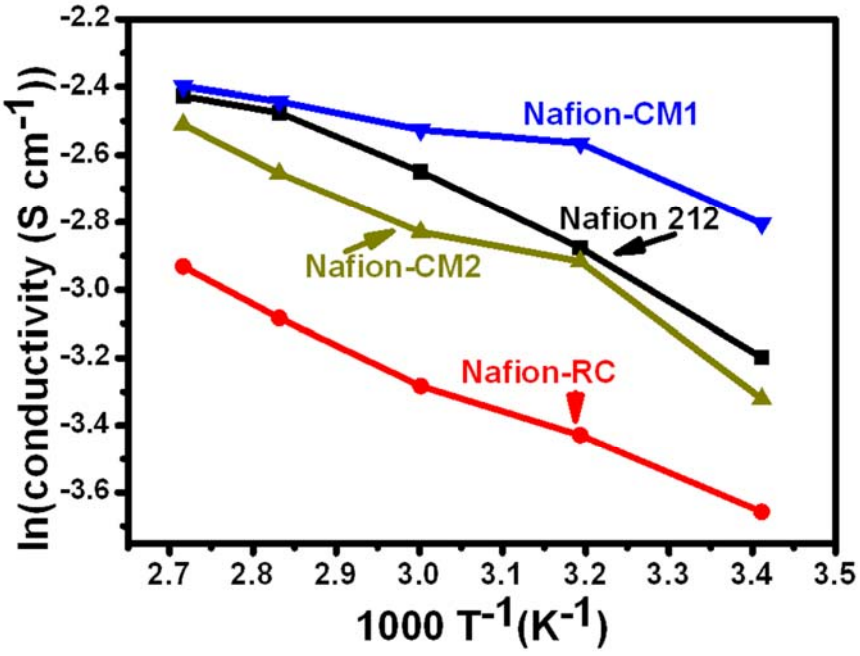

Figure 7. Proton conductivities at different temperatures of Nafion-based membranes.

The approaches to enhance the proton conduction with increases in the hydrophilic domain sizes of Nafion-based membranes usually results in increases in fuel (methanol and hydrogen) permeability of the membranes.[53] The trade-off properties of proton conductivity and fuel permeability are critical for the Nafion-based membranes, especially for the application in direct-methanol fuel cells (DMFC). Our previous paper[21] has reported the approach to simultaneously increase the proton conductivity and depress the methanol permeability of Nafion membranes with Fe_3O_4 nanoparticle-anchored and Nafion-functionalized CNTs. The similar attractive property has also been observed with the Nafion-CM1 membrane in this work. The recast Nafion-RC membrane has a methanol permeability of $14.6*10^{-7}$ cm^2 s^{-1}, which is relatively low compared to the reported values due to the relatively large thickness of Nafion-RC prepared in this work. The methanol permeability recorded with Nafion-CM1 decreases to $8.6*10^{-7}$ cm^2 s^{-1}, indicating formation of composite membrane is effective to reduce the methanol crossover of Nafion-based membranes. It is noteworthy that the

methanol permeability of Nafion-CM1 membrane is much lower than the value ($15.0*10^{-7}$ cm^2 s^{-1}) recorded with Nafion 117, even the thickness of Nafion 117 is almost twice of the thickness of Nafion-CM1. The above-mentioned SAXS data also suggests that distortion of ionic channels could attribute to the reduction of methanol permeability. Reduction of the methanol permeability of proton exchange membranes with electrospun nanofibers has been reported[32,37,42] and attributed to the reduction of swelling of Nafion associated with the presence of nanofiber mats. Nevertheless, the reported membranes still exhibited reduced proton conductivities. As a result, the simultaneous increase of proton conductivity and decrease of methanol permeability of Nafion-CM1 demonstrate a high selectivity (the ratio of proton conductivity over methanol permeability), which is 2.4-folds of the value of Nafion-RC. The high proton conductivity and selectivity of Nafion-CM1 membrane warrant its high performance for hydrogen and direct-methanol fuel cells. The results are to be presented and discussed below.

Single cell performance employing Nafion-CM1 membrane

The relatively high proton conductivity of the Nafion-CM1 membrane indicates its suitability of application for proton exchange membrane fuel cells. In the H_2/O_2 single cell test (**Figure 8**) Nafion-CM1 shows a maximum power density of 700 mW cm^{-2} which is larger than the values found with Nafion-RC (400 mW cm^{-2}) and Nafion 212 (500 mW cm^{-2}) (Table 2). It is noteworthy that Nafion-CM1 membrane shows a low activation resistance at the low current density region. As a result, Nafion-CM1 shows a high value (960 mA cm^{-2}) of current density at 0.6 V. The value is about twice of the values found with Nafion-RC and Nafion 212 membranes. The single cell tests using air as the feeding oxidant (H_2/air fuel cell test) have also been performed. Nafion-CM1 membrane shows about 50% increase in the maximum power density compared to the data recorded with Nafion-RC and Nafion 212. The performance drop associating with the single cell employing air as the oxidant could be

attributed to the reduced oxidant supply. The nitrogen in the fed air might accumulate in the gas diffusion layer (GDL) of the cathode so as to reduce the oxygen diffusion rate through the GDL to the cathode.[54-56] The extent of cell performance drop in this work is comparable to the values reported previously.[57]

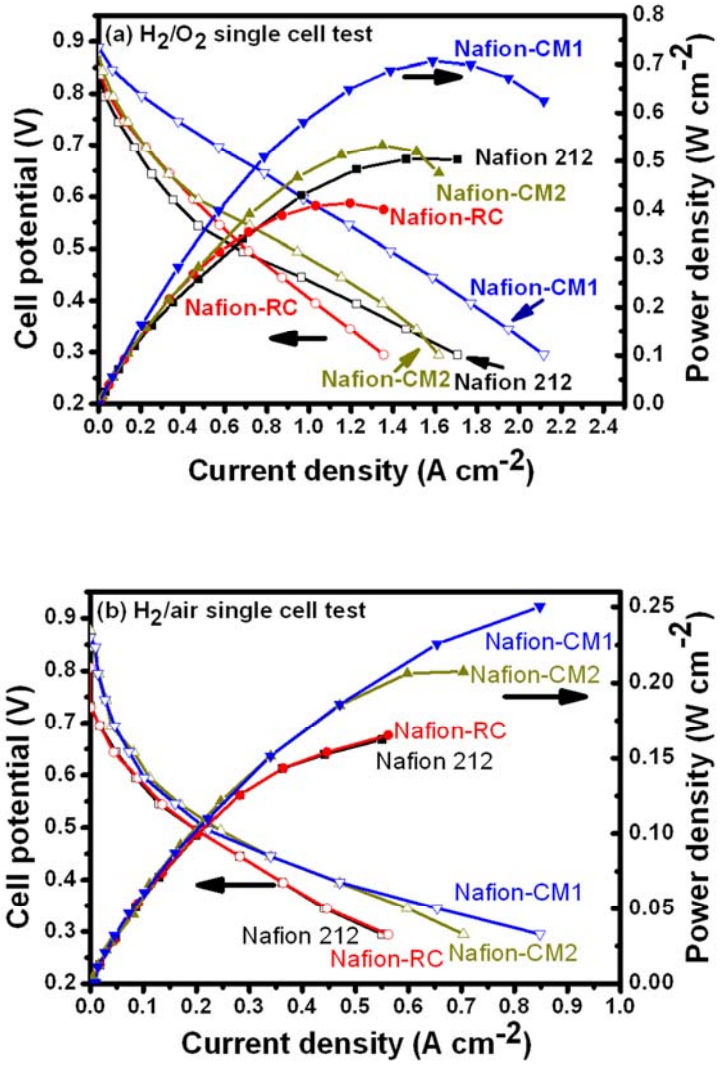

Figure 8. Plots of single cell tests of Nafion-based membrane s at 65 °C. (a) H_2/O_2 single cell tests and (b) H_2/air single cell tests.

Formation of Nafion composite membrane with PVDFNF-Nafion simultaneously results in an increase in the proton conductivity and a decrease in the methanol permeability. As a

result, Nafion-CM1 membrane shows a high membrane selectivity (proton conductivity/methanol permeability) which is 4.7-fold of the value of Nafion-RC and 2.5-fold of that of Nafion 117. The high selectivity of Nafion-CM1 implies its high performance for application in DMFC. **Figure 9** shows the DMFC performance of the single cells employing the Nafion-based membranes. With a 2M methanol solution as the fuel, the maximum power density recorded with Nafion-CM1 is 83 mW cm^{-2}, which is about 30% higher than the value (60 mW cm^{-2}) recorded with the commercial Nafion 117 membrane (**Table 3**). The current density at 0.2 V found with Nafion-CM1 and Nafion 117 is 425 and 320 mA cm^{-2}, respectively. Moreover, the low methanol permeability of Nafion-CM1 makes it possible to operate the single cell tests with methanol fuel solutions in high concentrations. For the single cell operated a 5M methanol solution as the feeding fuel (**Figure 9b**), the maximum power density and current density at 0.2 V recorded with Nafion-CM1 membrane have been further enhanced to 122 mW cm^{-2} and 615 mA cm^{-2}, respectively. The modification approach on Nafion membranes in this work has demonstrated significant improvements of the membrane properties and the corresponding fuel cell performance.

Table 3. Direct methnaol fuel cell tests of the Nafion-based membranes at 70 ºC.

Membrane	Proton conductivity at 20 ºC (mS cm^{-1})	Methanol permeability (*10^{-6} cm^2 s^{-1})	Relative selectivity	Direct methanol fuel cell test at 2M methanol			Direct methanol fuel cell test at 5M methanol		
				OCV (V)	Maximum power density (mW cm^{-2})	Current density at 0.2 V (mA cm^{-2})	OCV (V)	Maximum power density (mW cm^{-2})	Current density at 0.2 V (mA cm^{-2})
Nafion-RC	22	1.46	1.0	0.62	55	275	-	-	-
Nafion-CM1	60	0.86	4.7	0.65	83	425	0.64	122	610
Nafion 117	42	1.50	1.9	0.64	60	320	-	-	-

Experimental

Materials

Nafion 212 and Nafion 117 membranes were received from DuPont Fluoroproducts. The product of Nafion dispersion D2020 received from the same company was used for

fabrication of recast Nafion-based membranes. D2020 has a polymer content of about 20 wt% with the mixture of water (34±2 wt%), isopropanol (46±2 wt%), and ethanol (< 2 wt%) as a solvent. The available acid capacity of the polymer is about 1.00 meq g^{-1}. PVDF was received from Elf Atochem Inc. USA (Kynar K-761). GMA was purchased from Aldrich Chemical Co. p-Maleimidobenzoic acid (MBA) was prepared according to the reported method.[58] Reagent grade solvents were used as received.

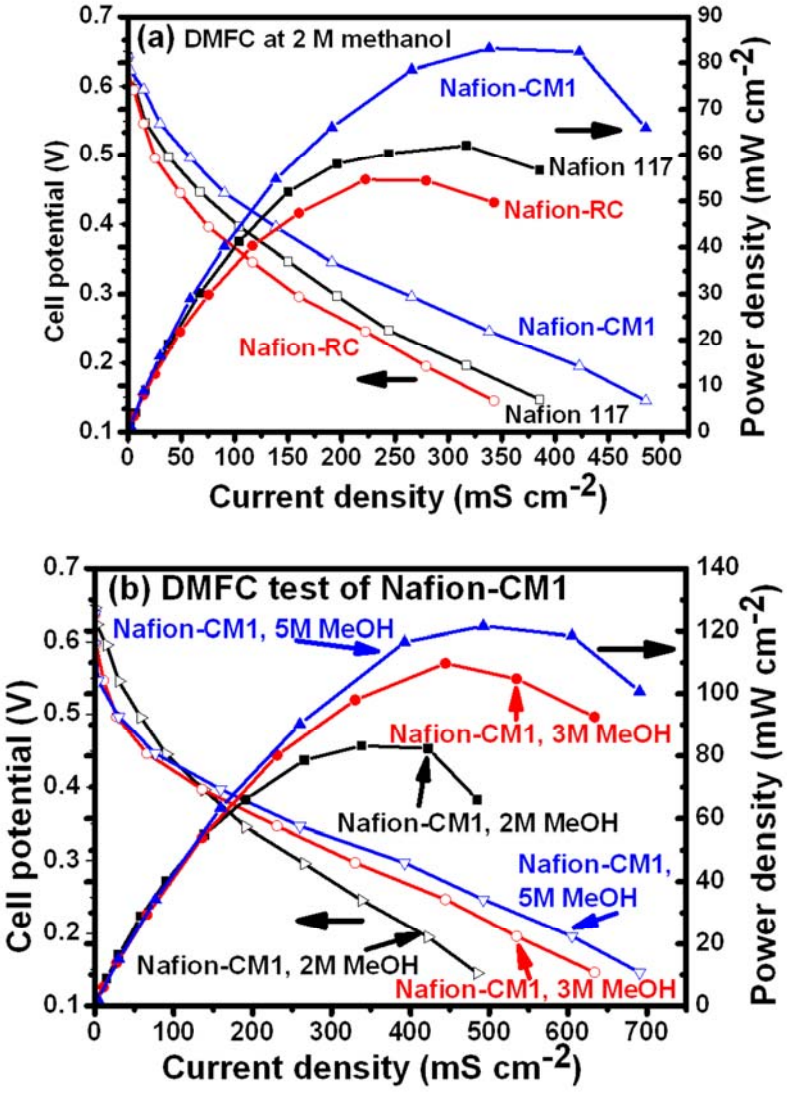

Figure 9. Plots of direct methanol fuel cell tests of (a) Nafion-based membranes at 2 M methanol and (b) Nafion-CM1 membrane at different methanol concentrations at 70 °C.

Instrumental methods

XPS spectra were recorded with an XPS instrument from Thermo VG-Scientific Co. (Model: Sigma Probe) using an Mg-Kα line as the radiation source. FTIR spectra were recorded with a Perkin Elmer Spectrum 2 FTIR instrument. SEM micrographs were recorded with a Hitachi S-4800 field-emission SEM. The samples chilled with liquid nitrogen were broken for cross-sectional observation. The samples were treated with a platinum deposition prior to SEM measurements. Mechanical properties of the membranes were measured with an instron machine (Instron model 5543 analyzer) with an elongation rate of 5 mm min^{-1} at ambient temperature. The Brüker Nanostar SAXS instrument equipped with a two-dimensional position-sensitive detector (Brüker AXS) with 512 × 512 channels and employed a radiation wavelength of 0.1541 nm was applied to in SAXS measurements. The proton conductivities of the hydrated membranes at about 95% relative humidity were measured with a method employing electrochemical impedance spectroscopies. The membrane clamped between two electrodes with an effective area of 1.0 cm^2 was applied to conductivity measurements with a 4-point-probe method. The membrane resistances were measured with a Solartron 1255B frequency response analyzer, which was equipped with a Solartron SI 1287 electrochemical interface. The oscillation amplitude and frequency range for the measurements were 10 mV and 10^2 to 10^6 Hz, respectively.

Preparation of electrospun PVDF nanofibers

A 17 wt% of PVDF solution in N,N-dimethylforamide was used as the feeding solution for the electrospinning process. A spinneret with a hole diameter of 0.33 mm was used. The electrospinning process was carried out at a voltage of 15 kV and a steady flow of about 25 μm min^{-1}. An aluminum target was put at a distance of 15 cm from the spinneret as the electrospun nanofibers collector. The collected nanofiber mats were dried under vacuum at room temperature for 24 h, and had a specific weight of about 0.95 mg cm^{-2}.

Preparation of PVDFNF-Nafion

Introduction of PGMA chains to PVDFNF surface was carried out with an ozone-mediated/surface-initiated polymerization of GMA.[59] PVDFNF was put in 1,4-dioxane, treated with a O_3/O_2 mixture gas stream for 15 min. and purged with a argon gas stream for 30 min., and then put in a solution of GMA in 1,4-dioxane (1.0 wt%). The polymerization of GMA was performed at 70 ^oC for 3 h under a nitrogen atmosphere. The samples were draw from the solution, washed in 1,4-dioxane under a ultrasonic bath, dried at room temperature for 24 h under vacuum to result in PVDFNF-PGMA. PVDFNF-PGMA samples were put in a MBA solution in 1,4-dioxane (0.1 wt%) . After reaction at 70 ^oC for 3 h, the samples were draw from the solution, washed in 1,4-dioxane under a ultrasonic bath, dried at room temperature for 24 h under vacuum to result in PVDFNF-MBA. PVDFNF-MBA samples were out in Nafion dispersion D2020, which was pretreated with a O_3/O_2 mixture gas stream for 15 min and purged with a argon gas stream for 30 min,[49] and reacted at 70 ^oC for 3 h under a nitrogen atmosphere. The samples were draw out, washed with a solution of methanol/water, mixture (30/70 in v/v) under an ultrasonic bath, dried at room temperature for 24 h under vacuum to result in PVDFNF-Nafion.

Preparation of composite membrane of Nafion and PVDFMNF-Nafion (Nafion-CM1)

Nafion-CM1 membrane was prepared by an impregnation process using PVDFNF-Nafion as a reinforcing material and Nafion dispersion D2020 as an impregnation solution. The fraction of the nanofiber in the composite membrane determined by gravimetric measurements is about 10 wt%. Nafion-CM2 membrane was obtained with the same manner using the neat PVDFNF as the reinforcing material. The membranes were then seuqencially immersed in deionic water at 80 ^oC for 1 h, $H_2O_{2(aq)}$ (3 wt%) at room temperature for 1 h, deionic water at 80 ^oC for 1 h, $H_2SO_{4(aq)}$ (1 M) at 80 ^oC for 1h, and deionic water at 80 ^oC for 1 h to result in the acid form of Nafion.

Single cell tests

Hydrogen fuel cell tests were carried out with a CHINO Fuel Cell Testing System (FC5100 series) at 65 ^{o}C. The gas flow rates of fuel and oxidants are 0.3 L min^{-1}. Both cathode and anode possessing 0.8 mg cm^{2} of Pt as the catalyst were prepared with a air-spraying method.[34] The electrodes and membrane were then sandwiched to form membrane electrode assembly (MEA) by hot pressing (784 N at 140 ^{o}C for 3 min). The active area of the membrane electrode assembly (MEA) used in the fuel cell tests was 5 cm^{2}. For DMFC tests,[21] the single cell performance was measured with a DMFC station (Model TEI-D160-1NBNNS, Tension Energy Inc., Taiwan) at 70 ^{o}C. For DMFC single cell tests, the catalyst of the anode and cathode was 5 mg cm^{-2} of Pt-Ru (1 : 1) and 5 mg cm^{-2} of Pt, respectively. The flow rate of the feeding fuel (MeOH aqueous solution) was 1 mL min^{-1}. The oxidant was oxygen at a flow rate of 0.2 L min^{-1}.

Conclusions

In this work, functionalization of PVDF nanofiber surface has been performed with a 3-step reaction to result in Nafion-functionalized PVDF electrospun nanofibers, which has been used as an alternative of Nafion nanofibers for preparation of Nafion composite membranes. The Nafion layer of PVDFNF-Nafion nanofibers provides interfacial compatibility between the nanofibers and Nafion matrix and contributes to induce the proton-conducting pathways along the nanofiber surfaces in the composite membrane. The nanofibers also improve the mechanical properties of the Nafion composite membrane, alter the crystalline structure of the Nafion matrix, and depress the methanol permeability of the membrane. As a result, the Nafion-CM1 composite membrane shows high performance in using as proton exchange membrane for both PEMFC and DMFC. The performance of the single cells employing the Nafion-CM1 composite membrane is superior over the data recorded with the commercial Nafion 212 and Nafion 117 membranes.

Acknowledgements

Financial supports on this work from the National Science Council, Taiwan (Grant: NSC 100-2221-E-007-127-MY3) are highly appreciated. We thank Professor Hsin-Lung Chen (National Tsing Hua University, Taiwan) for SAXS analysis. The assistance from the Fuel Cell Center of Yuan Ze University (Taiwan) on the PEMFC instrumentation and the R&D Center for Membrane Technology of Chung Yuan Christian University (Taiwan) on the DMFC facility is highly appreciated.

References

1. C. H. Park, C. H. Lee, M. D. Guiver and Y. M. Lee, *Prog. Polym. Sci.*, **2011**, *36*, 1443-1498.
2. H. Zhang and P. K. Shen, *Chem. Soc. Rev.*, 2012, **41**, 2382-2394.
3. H. Zhang and P. K. Shen, *Chem. Rev.*, 2012, **112**, 2780-2832.
4. Y. L. Liu, *Polym. Chem.*, 2012, **3**, 1373-1383.
5. N. Li, S. Y. Lee, Y. L. Liu, Y. M. Lee and M. D. Guiver, *Energy Environ. Sci.*, 2012, **5**, 5346-5355.
6. L. Wu, Z. Zhang, J. Ran, D. Zhou, C. Li and T. Xu, *Phys. Chem. Chem. Phys.*, 2013, **15**, 4870-4887.
7. S. Takamuku and P. Jannasch, *Macromol. Rapid Commun.*, 2011, **32**, 474-480.
8. B. Bae, T. Yoda, K. Miyatake, H. Uchida and M. Watanabe, *Angew. Chem. Int. Ed.*, 2010, **49**, 317-320.
9. Y. H. Su, Y. L. Liu, D. M. Wang, J. Y. Lai, Y. M. Sun, S. D. Chyou and W. T. Lee, *J. Membr. Sci.*, 2010, **349**, 244-250.
10. N. Li, D. S. Hwang, S. Y. Lee, Y. L. Liu, Y. M. Lee and M. D. Guiver, *Macromolecules*, 2011, **44**, 4901-4910.

11. B. P. Tripathi and V. K. Shahi, *Prog. Polym. Sci.*, 2011, **36**, 945-979.
12. M. Amirinejad, S. S. Madaeni, E. Rafiee and S. Amirinejad, *J. Membr. Sci.*, 2011, **377**, 89-98.
13. Y. H. Su, Y. L. Liu, Y. M. Sun, J. Y. Lai, D. M. Wang, Y. Gao, B. Liu and M. D. Guiver, *J. Membr. Sci.*, 2007, **296**, 21-28.
14. C. H. Rhee, H. K. Kim, H. Chang and J. S. Lee, *Chem. Mater.*, 2005, **17**, 1691-1697.
15. P. Bébin, M. Caravanier and H. Galiano, *J. Membr. Sci.*, 2006, **278**, 35-42.
16. R. Kannan, B. A. Kakade and V. Pillai, *Angew. Chem. Int. Ed.*, 2008, 47, 2653-2656.
17. R. Kannan, M. Parthasarathy, S. U. Maraveedu, S. Kurungot and V. Pillai, *Langmuir*, 2009, **25**, 8299-8305.
18. Y.L. Liu, Y. H. Su, C. M. Chang, Suryani, D. M. Wang and J. Y. Lai, *J. Mater. Chem.*, 2010, **20**, 4409-4416.
19. Suryani, C. M. Chang, Y. L. Liu and Y. M. Lee, *J. Mater. Chem.*, 2011, **21**, 7480-7486.
20. C. M. Chang, H. Y. Li, J. Y. Lai and Y. L. Liu, *RSC Advances*, 2013, **3**, 12895-12904.
21. Z. M. Huang, Y. Z. Zhang, M. Kotaki and S. Ramakrishna, *Composites Sci. Technol.*, 2003, **63**, 2223-2253.
22. J. Weber, *ChemSusChem*, 2010, **3**, 181-187.
23. J. Choi, K. M. Lee, R. Wycisk, P. N. Pintauro and P. T. Mather, *Macromolecules*, 2008, **41**, 4569-4572.
24. J. Choi, R. Wycisk, W. Zhang, P. N. Pintauro, K. M. Lee and P. T. Mather, *ChemSusChem,* 2010, **3**, 1245-1248.
25. J. Choi, K. M. Lee, R. Wycisk, P. N. Pintauro and P. T. Mather, *J. Mater. Chem.*, 2010, **20**, 6282-6290.
26. J. Choi, K. M. Lee, R. Wycisk, P. N. Pintauro and P. T. Mather, *J. Electrochem. Soc.*, 2010, **157**, B914-B919.

27. Y. Yao, B. Guo, L. Ji, K. H. Jung, Z. Lin, M. Alcoutlabi, H. Hamouda and X. Zhang, *Electrochem. Commun.*, 2011, **13**, 1005-1008.

28. W. Liu, S. Wang, M. Xiao, D. Han and Y. Meng, *Chem. Commun.*, 2012, **48**, 3415-3417.

29. D. S. Liu, J. N. Ashcraft, M. M. Mannarino, M. N. Silberstein, A. A. Argun, G. C. Rutledge, M. C. Boyce and P. T. Hammond, *Adv. Funct. Mater.*, 2013, **23**, 3087-3095.

30. M. M. Hasani-Sadrabadi, I. Shabani, M. Soleimani and H. Moaddel, *J. Power Sources*, 2011, **196**, 4599-4603.

31. D. M. Yu, K. Yoon, Y. J. Yoon, T. H. Kim, J. Y. Lee and Y. T. Hong, *Macromol. Chem. Phys.*, 2012, **213**, 839-846.

32. J. H. Seol, J. H. Won, M. S. Lee, K. S. Yoon, Y. T. Hong and S. Y. Lee, *J. Mater. Chem.*, 2012, **22**, 1634-1642.

33. H. Y. Li and Y. L. Liu, *J. Mater. Chem. A*, 2013, **1**, 1171-1178.

34. T. Tamura and H. Kawakami, *Nano Lett.*, 2010, **10**, 1324-1328.

35. T. Tamura, R. Takemori and H. Kawakami, *J. Power Sources*, 2012, **217**, 134-141.

36. S. W. Choi, Y. Z. Fu, Y. R. Ahn, S. M. Jo and A. Manthiram, *J. Power Sources*, 2008, **180**, 167-171.

37. J. R. Lee, N. Y. Kim, M. S. Lee and S. Y. Lee, *J. Membr. Sci.*, 2011, **367**, 265-272.

38. J. B. Ballengee, P. N. Pintauro, *Macromolecules*, 2011, **44**, 7307-7314.

39. Y. Yao, Z. Lin, Y. Li, M. Alcoutlabi, H. Hamouda and X. Zhang, *Adv. Energy. Mater.*, 2011, **1**, 1133-1140.

40. Y. Yao, L. Ji, Z. Lin, Y. Li, M. Alcoutlabi, H. Hamouda and X. Zhang, *ACS Appl. Mater. Interfaces*, 2011, **3**, 3732-3737.

41. I. Shabani, M. M. Hasani-Sadrabadi, V. Haddadi-Asi and M. Soleimani, *J. Membr. Sci.*, 2011, **368**, 233-240.

42. J. B. Ballengee and P. N. Pintauro, *J. Membr. Sci.*, 2013, **442**, 187-195.

43. K. M. Lee, J. Choi, R. Wycisk, P. N. Pintauro andP. T. Mather, *ECS Transactions*, 2009, **25**, 1451-1458.

44. R. Bajon, S. Balaji and S. M. Guo, *J. Fuel Cell Sci. Technol.* 2009, **6**, 031004 (6 pages).

45. B. Dong, L. Gwee, D. Salas-de la Cruz, K. I. Winey and Y. A. Elabd, *Nano Lett.*, 2010, **10**, 3785-3790.

46. Y. Chen, J. Guo and H. Kim, *React. Funct. Polym.*, 2010, **70**, 69-74.

47. C. Nah, K. U. Jeong, Y. S. Lee, S. H. Lee, M. M. A. Kader, H. K. Lee and J. H. Ahn, *Polym. Int.*, 2013, **62**, 375-381.

48. C. M. Chang and Y. L. Liu, *Carbon*, 2012, **48**, 1289-1297.

49. J. A. Prince, G. Singh, D. Rana, T. Matsuura and T. S. Shanmugasundaram, *J. Membr. Sci.*, 2012, **397-398**, 80-86.

50. C. S. Tsao, H. L. Chang, U. S. Jeng, J. M. Lin and T. L. Lin, *Polymer*, 2005, **46**, 8430-8437.

51. R. Kannan, M. Parthasarathy, S. U. Maraveedu, S. Kurungot and V. K. Pillai, *Langmuir*, 2009, **25**, 8299-8305.

52. F. Wang, M. Hickner, Y. S. Kim, T. A. Zawodzinski and J. E. McGrath, *J. Membr. Sci.*, 2002, **197**, 231-242.

53. D. R. Sena, E. A. Ticianelli, V. A. Paganin and E. R. Gonzalez, *J. Electroanal. Chem.*, 1999, **477**, 164-170.

54. J. Shim, H. Y. Ha, S. A. Hong and I. H. Oh, *J. Power Sources*, 2002, **109**, 412-417.

55. Y. Bultel, K. Wiezell, F. Jaouen, P. Ozil and G. Lindbergh, *Electrochim. Acta*, 2005, **51**, 474-488.

56. Y. Lim, D. Seo, S. Lee, H. Jang, H. Ju, A. Jo, D. Kim and W. Kim, *Int. J. Hydrogen Energy*, 2013, http://dx.doi.org/10.1016/j.ijhydene.2013.05.165.

57. Y. L. Liu and Y. H. Wang, *J. Polym. Sci. Part A: Polym. Chem.* 2004, **42**, 3178-3188.

58. C. Y. Tu, Y. L. Liu, K. R. Lee and J. Y. Lai, *J. Membr. Sci.*, 2006, **274**, 47-55.

Figure caption

Figure 1. Synthetic route of Nafion-functionalized PVDF nanofibers (PVDFNF-Nafion) and preparation of Nafion-CM1 composite membrane.

Figure 2. Characterization of surface-functionalized PVDF nanofibers. (a) XPS wide-scan spectra, (b) XPS C_{1s} core-level spectra, and (c) FTIR spectra.

Figure 3. SEM micrographs of surface-functionalized PVDF nanofibers.

Figure 4. SEM micrographs of Nafion-based membranes at a cross-sectional view.

Figure 5. (a) Stress-strain curves of Nafion-based membranes recorded with an Instron; (b) Pictures of the Nafion-CM1 and Nafion-CM2 samples before and after Instron tests; and (c) SEM micrographs of the Nafion-CM1 and Nafion-CM2 samples before and after Instron tests.

Figure 6. Small angle X-ray scattering spectra of Nafion-based membranes.

Figure 7. Proton conductivities at different temperatures of Nafion-based membranes.

Figure 8. Plots of single cell tests of Nafion-based membrane s at 65 ^{o}C. (a) H_2/O_2 single cell tests and (b) H_2/air single cell tests.

Figure 9. Plots of direct methanol fuel cell tests of (a) Nafion-based membranes at 2 M methanol and (b) Nafion-CM1 membrane at different methanol concentrations at 70 ^{o}C.